AN INVESTIGATION INTO THREE DIMENSIONAL TURBULENT FLOW OF NEWTONIAN LIQUID IN STIRRED TANKS MIXERS

Prof. Dr. Ihsan Y. Hussian
Mech. Eng. Dept./College of Eng.
University of Baghdad / Baghdad-Iraq

Nizar Jawad Hadi
Electrical Eng. Dept./College of Eng.
University of Babylon/ Babylon-Iraq

ABSTRACT:

The present work is concerned with the theoretical and experimental investigation of flow pattern of Newtonian fluid in liquid mixing process in stirred tank with flat blade impeller. A three-dimensional model for mixing process was simulated. The effected parameters are rotation speed and impeller diameter. Continuity, momentum, and turbulent equations were solved by ANSYS package software 5.4 code with FLOTRAN/CFD based on Finite Element method. In the experimental work, two visualization methods are used in this work, the first method is the acid-base reaction visualization method and the second is the particle distribution visualization method. Different chemical materials were used in the first method, $NaOH$ as a base, H_2SO_4 as acid and Methyl red as indicator, while polymer particles were used in the second method. The results of 3D model showed that the speed rotation directly affected the mixing zones, where the speed reduction by half decreasing the mixing zones approximately by half. Also the impeller diameter increasing clearly affected the mixing process where the mixing zones concentrated directly above and below the impeller. In the experimental work, the acid-base reaction visualization method showed that the mixing zones decreased due to the rotation speed reduction depend on the red and yellow colors, which describe the good mixing and poor mixing zones respectively. The mixing zones were concentrated directly above and below the impeller due to the impeller diameter increasing,. The particles distribution method showed that the mixing zones decreased due to the speed reduction, while the mixing zones concentrated directly above and below the impeller due to the impeller diameter increasing. The results showed a good agreement between the theoretical and experimental works in studying the effect of rotating speed, and impeller diameter .

الخلاصة :

هذا البحث يتعلق بالدراسة العملية والنظرية لجريان سائل نيوتيوني أثناء عملية خلطه باستخدام تأثير عوامل مختلفة في خزان يدور فيه السائل بواسطة ريشة مسطحة. تصميم ثلاثي الأبعاد لعملية الخلط تمت محاكاته في هذا البحث. العوامل المؤثرة التي استخدمت في التصميم ثلاثي الأبعاد هي السرعة ألد ورانية، قطر الريشة. معادلة الاستمرارية، الزخم، والاضطراب تم حلها بواسطة Ansys package FLOTRAN/CFD والتي استندت إلى طريقة العناصر المحددة F .E. method. في الجانب العملي من البحث ، طريقتان لتصوير جريان السائل استخدمت في هذا البحث الطريقة الأولى هي طريقة تصوير تفاعل الحامض مع القاعدة والثانية هي طريقة تصوير توزيع الجزيئات. مواد كيميائية مختلفة استخدمت في الطريقة الأولى هيدروكسيد الصوديوم NAOH كقاعدة، حامض الكبريتيك H_2SO_4 كحامض، والمثيل الأحمر Methely red ككاشف بينما جزيئات بلاستيكية استخدمت في الطريقة الثانية .النتائج للتصميم ثلاثي الأبعاد أظهرت إن السرعة ألد ورانية أثرت بشكل مباشر على مناطق الخلط حيث أن تقليل السرعة إلى النصف أدى إلى تقليل مناطق الخلط تقريبا إلى النصف وبشكل واضح زيادة القطر أثرت على عملية الخلط. في الجانب العملي طريقة تصوير تفاعل الحامض مع القاعدة أظهرت إن مناطق الخلط قلت بسبب نقصان السرعة ألد ورانية اعتمادا على توزيع الألوان الأصفر والأحمر والتي توصف مناطق الخلط الجيدة والغير جيدة على التوالي. مناطق الخلط تتركز مباشرة فوق وتحت الريشة بسبب زيادة القطر. طريقة توزيع الجزيئات أظهرت إن مناطق الخلط تقل نتيجة لتقليل السرعة الدورانية، بينما تتركز فوق وتحت الريشة بسبب زيادة القطر . النتائج أظهرت توافق جيد بين الجانب النظري و العملي في دراسة تأثير السرعة ألد ورانية و قطر الريشة.

KEYWORDS: Mixers, Newtonian liquid, Turbulent, Three Dimensional

INTRODUCTION:

Mixing is generally considered as a complex subject, but its essence is quit simple: related stretching and folding of fluid elements. Stirred tanks are widely used in mixing process for blending, liquid-liquid dispersion, suspension formation, heat transfer, mass transfer and chemical reactions. Efficient mixing is crucial to the outcomes of all of these processes. For these applications, poor mixing can have serious consequences such as excessive by product formation, inconsistent product quality in blended products, wide particle size distributions in crystallization processes, and slow mass transfer rates in bioreactors, (Ottino, 1989). (Verzico et al, 2000), studied the flow induced by an impeller in a cylindrical tank, and showed that the combination of the Immersed Boundary " IB " procedure with DNS and LES (Large Eddy Simulation), simulations can efficiently be used for the accurate prediction and analysis of many technologically relevant flows.(Kresta et al, 1991), showed that the three dimensional simulations allow a realistic treatment of the baffles, where details of the predicted behavior of turbulence Kinetic energy and dissipation rate are in quantitative agreement with the available data. (Szalai et al, 2002), stated that the ORCA uses Galerkin least-squares finite element technology, novel approach to computer aided modeling and optimizing mixing process. Computer aided mixing, modeling, and analysis involves Lagrangian and Eulerian analysis for relative fluid stretching, and energy dissipation concepts for

laminar and turbulent flows. High quality, conservative accurate, fluid velocity, and continuity solutions are required for determining mixing quality. The present work studied the flow patterns and mixing process in the turbulent flow of the liquid stirred mixer. The ANSYScode/FLOTRANE CFD that based on finite element method was used for theoretical work

NUMERICAL SIMULATION:

Continuity, momentum, and two turbulence equations were solved in the present work these equation are respectively as follows (Nizar 2006):

$$(1) \qquad \frac{\partial(V_y)}{\partial y}+\frac{\partial(V_z)}{\partial z}=0 \qquad \frac{\partial(V_x)}{\partial x}+$$

$$(2) \qquad =\rho\{g\}-\nabla P_{abs}+\mu\nabla^2\{V\} \;\; \rho\frac{D\{V\}}{Dt}+2\rho\{\omega\}*\{V\}+\rho\{\omega\}*\{\omega\}*\{r\}$$

$$\rho\frac{\partial\varepsilon}{\partial t}+\rho\frac{(\partial V_x\kappa)}{\partial x}+\rho\frac{\partial V_y\kappa}{\partial y}+\rho\frac{\partial V_z\kappa}{\partial z}=$$

$$\frac{\partial}{\partial x}\left(\frac{\mu_t}{\sigma_\kappa}\frac{\partial\kappa}{\partial x}\right)+\frac{\partial}{\partial y}\left(\frac{\mu_t}{\sigma_\kappa}\frac{\partial\kappa}{\partial y}\right)+\frac{\partial}{\partial z}\left(\frac{\mu_t}{\sigma_\kappa}\frac{\partial\kappa}{\partial z}\right)+\mu_t\phi-\rho\varepsilon+$$

$$(3) \qquad \frac{C_4\beta\mu_t}{\sigma_t}\left(g_x\frac{\partial T}{\partial x}+g_y\frac{\partial T}{\partial y}+g_z\frac{\partial T}{\partial z}\right)$$

$$\rho\frac{\partial\varepsilon}{\partial t}+\rho\frac{\partial V_x\varepsilon}{\partial x}+\rho\frac{\partial V_y\varepsilon}{\partial y}+\rho\frac{\partial(V_z\varepsilon)}{\partial z}=$$

$$\frac{\partial}{\partial x}\left(\frac{\mu_t}{\sigma_\varepsilon}\frac{\partial\varepsilon}{\partial x}\right)+\frac{\partial}{\partial y}\left(\frac{\mu_t}{\sigma_\varepsilon}\frac{\partial\varepsilon}{\partial y}\right)+\frac{\partial}{\partial z}\left(\frac{\mu_t}{\sigma_\varepsilon}\frac{\partial\varepsilon}{\partial z}\right)+C_1\mu_t\frac{\varepsilon}{\kappa}\phi-C_2\rho\frac{\varepsilon^2}{\kappa}$$

$$\frac{C_1C_\mu(1-C_3)\beta\rho\kappa}{\sigma_t}\left(g_x\frac{\partial T}{\partial x}+g_y\frac{\partial T}{\partial y}+g_z\frac{\partial T}{\partial z}\right)$$

(4)

During the present work F.E method (Finite Element) was used and the numerical simulation was carried out by commercial software ANSYS 5.4 code, which is based on this method.

Tetrahedral grid and cylindrical coordinate of element FLUID142 is suggested for modeling present problem. The flow is assumed to be Newtoian, incompressible, single phase, and turbulent.

The boundary conditions applied for mixing process are as following:.

1-No-slip condition at the bottom of the tank, Vx = 0, Vz = 0, and Vy =0

2-No-slip condition at the wall of the tank, Vx = 0, Vz = 0, and Vy = 0).

3-Flat free slip conditions at the top of the tank.

4-Vx = 0.157 m/S., Vz = 0, Vy = 0, at the tip of the impeller, this velocity is changes to 0.0785 m/S. in the first case of study.

5-κ = .5, ε = 1, at the tip of the impeller.

The dimensions of the tank is 0.09 m in diameter, 0.12 m high, and has a liquid height of 0.105 m. its bottom has a flat plate shape, and the shaft is 0.005m in diameter. Six radial-pumping impellers with an outer diameter of 0.03 m, width .012m, and .002m thickness are positioned at 0.046m above the tank bottom, the impeller and shaft rotate at 100rpm. The fluid has a density of 1000 kg/m^3, a viscosity of 0.001 kg/m-s, and the flow is turbulent. The property of the fluid used in the present work is for water.

A segregated, sequential solution algorithm is used. This means that element matrices are formed, assembled and the resulting system solved for each degree of freedom separately. Development of the matrices proceeds in two parts. In the first, the form of the equations is achieved and an approach take towards evaluating all the terms. Next, the segregated solution algorithm is outlined and the element matrices are developed from the equations.

EXPERIMENTAL WORK:

A visualization technique based on an acid-base reaction and on particle distribution is used in the present experimental work to investigate the flow pattern qualitatively. This is important to validate the theoretical work. The experimental apparatus consists of many components, mixer, rotor, vessel, regulator, cover of the vessel, needle, chemical material, polymer particle, digital camera, and analog speed meter. It is used to test the flow pattern depending on colors in acid-base visualization method and on particle distribution according to the flow trajectories in the particle visualization method. Acid- base reaction visualization method is a visualization technique based on an acid-base neutralization reaction, also exploits the size and shape of segregated regions in the mixing tank. A soluble, PH-sensitive indicator, that appears yellow in base media and red in acidic media is added to each of the fluids. When the mixture components come into contact during the mixing process, the neutralization reaction instantaneously proceeds at the interface and a color change occurs.

Particles distribution visualization method used ellipsoidal polymer particles with longitudinal port. The particles in this test illustrate the flow trajectories in stirred tank.

NUMERICAL RESULTS:

The effects of two parameters on flow pattern and mixing process in stirred tank were studied. These parameters are as follows:

1-Rotation speed, which is decreased from 100 rpm to 50 rpm

2-Impeller diameter, which is increased from 0.03m to .045m.

The effect of rotating speed results in **Fig.1** shows the same shapes of the radial velocity general and the vertical velocity reduced by half, due to the rotating speed reduction. **Fig.2** shows that the axial velocity is decreased from 0.458 to 0.216m/s or about 53 %, due to the same reason. The same general contour shapes in two pictures are occurred. These results closely follow the results of Verzico et al, 2000. **Fig. 3** illustrates the same behavior of azimuthel velocity contours in general, a small change in contours shapes of the second graph above and below the impeller is occurred. The azimuthel velocity decreased from0.186 to 0.089m/s or about 50 %, due to the speed reduction from 0.157 to 0.0785m/s. **Fig. 4** illustrates the two recirculation flow in the regions above and below the impeller in each pictures. The recirculations in **Fig.4, b** above the impeller is shifted up and towards the tank wall, due to the speed reduction. Agreement of these results with that Verzico et al, 2000,. The centers of loops below the impeller are closer to the rotating shaft than the loops above the impeller in two pictures. The effect of impeller diameter in **Figs. 5, a, b** and **6, a, b** show that the meridional plan is roughly divided into two halves by the radial jet flow from the impeller. It can be noted that the two recirculations are not symmetric owing to the different boundary conditions on the upper and lower horizontal surfaces. An important effect of lower no-slip wall is the strongly positive vertical velocity in the lower half of the domain in the region close to the shaft, see **Fig. 6, a, b**. This effect is characteristic of wall-bounded rotating flows. It causes the fluid to be pushed radially inward at the plate, see **Fig.5, a, b** and axially upward at the axis of rotation as shown in **Fig.6, a, b**. Because of mass conservation, a vertical ascending fluid column at the axis induces a descending current at the external radial wall, thus reinforcing the lower-half recirculation with respect to the upper one. This is also well evidenced by the radial jet that dose not point exactly in the radial direction, but rather has a position vertical velocity close to the blade region and then a weakly negative vertical velocity. The radial velocity is increased by 133 %, while the axial velocity is increased by 57 % in general and particularly above the impeller near the surface and directly below the impeller. **Fig.7, a, b** indicates the effect of impeller diameter increasing on the shapes of contours. The maximum azimuthal velocity is increased from 0.186 to 0.296m/s or about

59 % and the first and second graphs are closely follow the results of Verzico et al, 2000. **Fig. 8** indicates the recirculations scale in the second graph are increased due to the impeller diameter increasing. The mixing flow is concentrated in front of blade directly below the impeller and above the impeller near the liquid surface also the recirculations above and below the impeller is shifted toward the tank wall

. The effect of rotating speed in **Fig. 9** at y= 0.03m shows that the regions near the shaft above and below the impeller a peak is observed. This is due to the large-scale recirculation that drives the fluid from the external radial region towards the axis, thus increasing the azimuthel velocity owing to the conservation of angular momentum. The maximum negative magnitude of radial velocity is reduced from –0.085 to –0.037m/s or about 53 %. Also the modes of axial velocity is similar to that in two dimensional model, and the maximum positive velocity magnitude is reduced from 0.255 to 0.13m/s or about 49 %, while the azimuthel velocity is decreasing from 0.04 to0.012m/s or about 70 %, due to the speed reduction. The positions of the maximum magnitude of radial and azimuthel velocities in the second graph are shifted towards the tank wall, due to the same reason**. Fig. 9, b** indicates zero velocity for all components at 0.035m distance from the rotating shaft, which illustrates poor mixing zone.**Fig.10** shows the behavior of radial, axial, and azimuthel velocities at centerline of the impeller. The decay of radial velocity in the second graph is slower than that in the first figure. The decay of azimuthal velocity is approximately occurred in the same profiles in the two graphs, and the peak of this velocity always in the limit of impeller radius end. The axial velocity is reduced and then increased in the two graphs. **Fig.11, a, b** shows that the decay of κ in the second picture is slower than that in the first one, due to the speed reduction. **Fig. 12, a, b** indicates that the decay of ε consist of two stages, the first one before 0.04m radial distance and the second one after 0.04m in the two Figs. Also the decay in the second picture is slower than that in the first one due to the speed reduction. Agreement is very good with the results of Kresta et al 1991. The effect of impeller diameter in **Fig.13** at y = 0.03m illustrates the radial profile of azimuthal, radial, axial velocity components at DT/3 and DT/2 respectively. The maximum magnitude of radial, axial, and azimuthal velocity is shifted towards the tank wall due to the impeller diameter increasing. The maximum negative magnitude of radial velocity is increased by194 %, the maximum positive magnitude of axial velocity is increased by 250 %, and the maximum positive magnitude of azimuthal velocity is increased by 72 %, due to the impeller diameter increasing. **Fig. 14** at y = 0.052m indicates the decay of radial velocity and the behavior of axial and azimuthal velocities on the centerline of impeller due to the impeller diameter increasing. The maximum magnitude of these velocities is shifted towards tank wall, and the axial velocity increased and then decreased toward the tank wall. In the second graph the curves behavior of

velocities is changed, and poor mixing zone is observed. **Fig. 15, a, b** shows the decay of κ on the impeller centerline in both impeller diameter, where the decay in the second graph consists of two stages. The first stage occurs before 0.035m radial distance and the second one occurs after 0.035m radial distance. **Fig. 16, a, b** indicates the decay of ε on the centerline of the impeller. The decay in the first and second graphs consists of two stages. The first stage in the first graph is ended at $\varepsilon = 0.2$, where the first stage in the second graph is ended at $\varepsilon = 0.35$, due to the impeller diameter increasing. It is useful to define zones in the stirred tank where average values of the turbulence quantities may be applied. Based on the results of these simulations, two zones have been defined. The first is the impeller discharge zone. The value of ε for this zone is virtually independent on D/D_T. The second zone comprises the remaining free volume of the tank, and reflects the influence of changing D/D_T. These results have a good agreement with that of Kresta et al, 1997

EXPERIMENTAL RESULTS:

Experimental results consist of two parts, the first one is acid-base reaction visualization and the second one is particle distribution visualization method. Acid-base Reaction Visualization Method in **Fig. 17, a, b** shows the effect of speed reduction on color change from yellow to red, and on the red color zones. In the second picture the changing from yellow to red color is slower than that in the first picture due to the speed reduction, and the color red zones in the second picture is smaller than that in the first one due to the same reason, which make the recirculation flow above and below the impeller shifted toward the rotating shaft.. The red color indicates the mixing zones and the yellow color indicates the poor mixing zones. The rotation speed reduction decreases the mixing zones and the mixing time, this also relates with the volume of the cylinder. **Fig.18, a, b** indicates the effect of impeller diameter increasing on the colors zones. The recirculation flow above and below the impeller associated with the impeller tips, and week mixing zones near the bottom of the tank and near the top surface of the liquid are observed in the second picture. The major different between these two pictures is that the strongly mixing occurs directly above and below the impeller, and the flow directed vertically above the impeller near the rotating shaft, due to the impeller diameter increasing in the second picture. **Figs. 17 and 18** show a good agreement with the results of Verzico et al, 1991 . Particles distribution visualization method in **Fig. 19, a, b** shows the effect of speed reduction on the particles distribution in the vessel, which indicates the same general behavior with reduction in the speed of the particles by half. Poor mixing zones above and below the impeller near the surface of liquid and near the bottom of the vessel are observed. Also the centers of circulation above and below the impeller are shifted toward the rotating shaft, due to the speed reduction. The mixing zones in the second picture are decrease according to the particles

distribution in the vessel**. Fig. 20, a, b** shows the effect of impeller diameter increasing on the particles distribution in the vessel. The centers of circulation are shifted with the impeller tip towards the vessel wall, due to the diameter increasing. The mixing zones are reduced in the second picture, due to the flow movement concentrated directly above and below the impeller. Comparison between numerical and acid-base reaction results in **Figs. 4 and 17** show the effect of speed reduction on the vectors distribution and the red and yellow color zones distribution respectively. The general behavior of vectors distribution and red color zones in these two figures is approximately the same, which indicates a good agreement between the numerical and experimental results. The mixing zones are decreasing in the second picture of each figure according to the vectors distribution and red color zones, respectively due to the rotation speed reduction. **Figs. 8 and 18** indicate the effect of the impeller diameter on the vectors distribution and red and yellow color zones distribution respectively. The general behavior of the vectors distribution and red color zones in these two figures is approximately the same, so the results of numerical simulation are closely following the results of experimental work. The mixing zones in the second picture of each figures are strongly concentrated above and bellow the impeller, and above the impeller near the rotating shaft. Comparison between numerical and particles distribution results in **Figs. 4 and 19** show the effect of the rotation speed reduction on the vectors and particles distribution respectively. The general behavior of vectors and particles in these two figures is approximately the same, which make a good agreement between the numerical and experimental results. According to the vectors distribution the mixing zones in the second picture of the first figure are decreased due to the velocity reduction, also the recirculation above and below the impeller are shifted toward the rotating shaft due to the same reason. The same behavior occurred in the second figure where the mixing zones are decreasing in the second picture as indicated from the particles distribution, also the recirculation flow above and below the impeller are shifted towards the rotating shaft due to the rotation speed reduction.

Figs. 8 and 20 show the effect of impeller diameter on the vectors and particles distribution respectively. The general behavior of the vectors and particles in these two figures is approximately the same, which makes the numerical results closely follow the experimental results. Depending on the vectors distribution the mixing zones in the two pictures of the first figure is approximately the same results in 3D model indicated that the negative radial velocity is decreased by 53 %, 54 %, and 35 % at 0.03m, 0.07m, and 0.09m heights respectively. The positive axial velocity is decreased by 49 %, 52 %, 45% at 0.03m, 0.07m, and 0.09m heights respectively. The azimuthal velocity is decreased by 50 %, keeps the same magnitude, and decreased by 60 % at 0.03m, 0.07m, and 0.09mheights respectively. Also the effect in axial velocity profiles indicated that the radial

velocitydecreased by 50 % at the centerline of impeller, and the negative axial velocity is decreased 30%, while the azimuthal velocity is decreased by 35 %.

CONCLUSIONS:

The Ansys/ FLOTRAN CFD, which uses Galerkin finite element technology, is a new approach to computer aided modeling and optimizing mixing processes. The Galerkin technique provides the basis of the confidence, accuracy, convergence, and stability of FLOTRAN. This method ensures extremely accurate solutions for the mixing process. The effect of speed rotation reduction in radial velocity profiles

The effect of impeller diameter increasing from 0.03m to 0.045m in the radial velocity results of 3D model indicated that the radial velocity is increased by 194 %, 180 %, and 100 % at 0.03m, 0.07m, and 0.09m heights respectively. The positive axial velocity is increased by 250 % at 0.03m height, and its negative magnitude is increased by 100 % at height 0,07m, while its negative magnitude is increased by 260 % at height 0.09m. The positive azimuthal velocity is increased by 59% at 0.03m height, and its positive magnitude is increased by 600 % at 0.09m height. Also the effect in axial velocity profiles indicated that the radial velocity is increased by 100 % at the centerline of impeller, and the negative axial velocity is increased by 166 %, while the positive azimuthal velocity is increased by 89 %. The qualitative results of the particle distribution and acid-base reaction visualization methods have a good agreement with the velocity vectors field in 3D -model simulation.

REFERENCES:

Kresta, S. M. and Wood, P. E. (1991), *Prediction of the Three-Dimensional Turbulent Flow in Stirred Tanks,* AICHE Journal, Vol. 37, No. 3. pp 448-458.

Mohammed Arab, A. A. M. (1981), Mixing *in Liquid –Liquid System*, Dissertation, Dept. of Chemical Engineering, University of Manchester Institute of Science and Technology.

Nagata, S. (1975), *Mixing Principles and Applications*, Wiley, London.

Nizar J.Hadi (2006) , *An Investigation Into Fluid Flow and Mixing Process in a Stirred Tank Newtonian Liquid Mixer*, Ph.D. Thesis, Mech. Eng. Dept., University of Baghdad

Ottino, J. M. (1989), The *Kinematics of Mixing: Stretching, Chaos and Transport*, Cambridge University Press, Cambridge.

Reddy, J. N. (1984), An *Introduction to the Finite Element Method*, textbook, Virginia Polytechnic Institute and State University.

Swanson, P. D. and Ottino, J. M. (1990), About *Mixing Technology*, Fluid Mech., 213: 227.

Szalai, E. S. and Muzzio, F. J. (2000), *Validation of the ORCA CFD Software For Three Stirred Tank Configuration* , Dept. of Chemical and Biochemical Engineering, Rutgers University. pp 1-9.

Verzico, R. Iaccarino, G. Fatica, M. and Orlandi, P. (2000), *Flow in an Impeller Stirred Tank Using anImmersed Boundary Method,* Center of Turbulence Research, Annual Research Briefs Bari, Italy. pp 251-260.

NOMENCLATUR:

Symboles	Definition	Units
N	Rotation Speed	rpm
Vx	Radial Velocity	m/s
Vz	Axial Velocity	m/s
Vy	Azimuthal Velocity	m/s
ε	Kinetic Energy Dissipation Rate	W
κ	Kinetic Energy	W

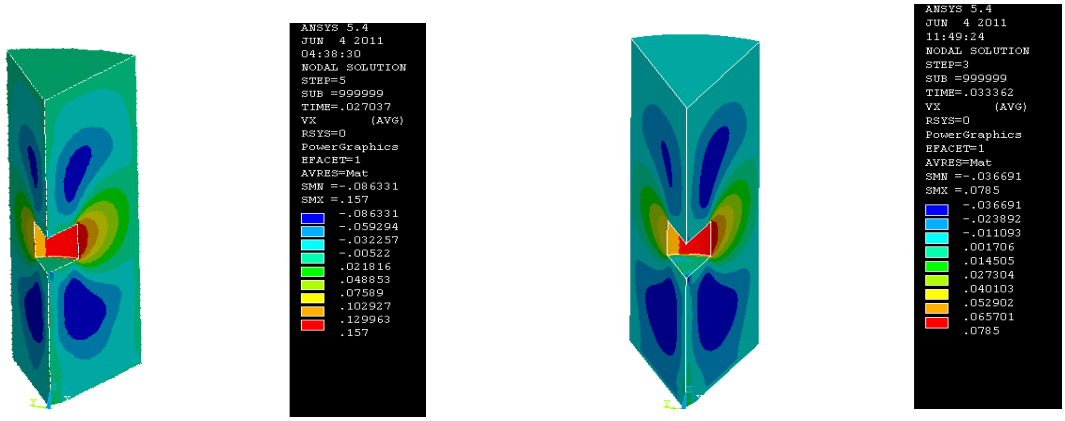

(a) (b)

Fig. 1. Effect of Rotating Speed (N) on Radial Velocity (Vx) Contours at, (a) N=100 rpm, (b) N=50 rpm..

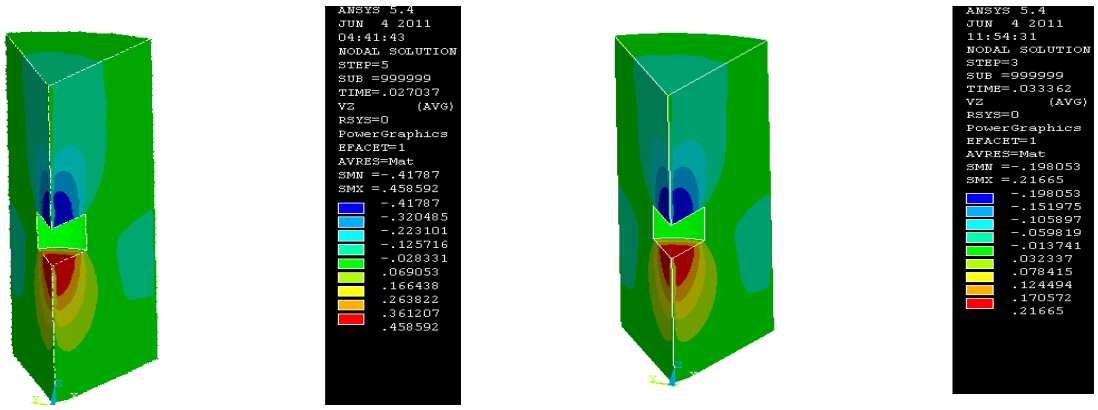

(a) (b)

Fig. 2. Effect of Rotating Speed (N) on Axial Velocity (Vz) Contours at, (a) N=100 rpm, (b) N=50 rpm.

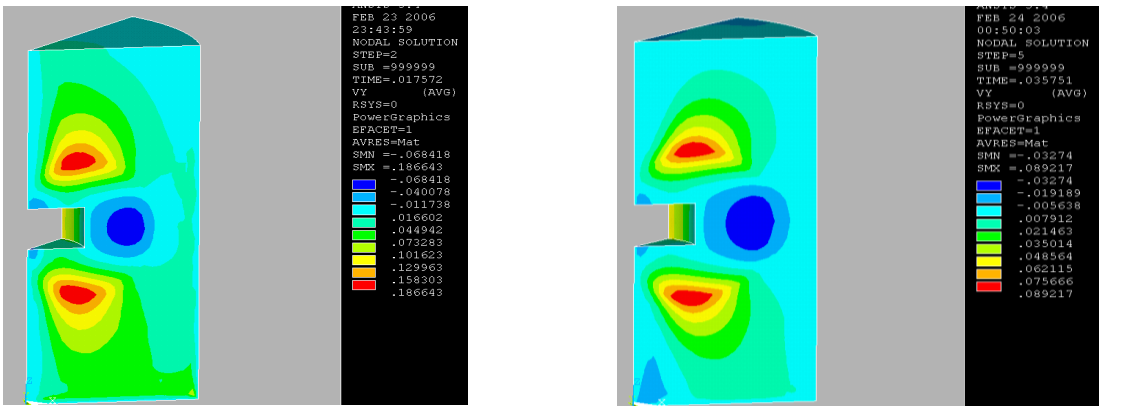

(a) (b)

Fig. 3. Effect of Rotating Speed (N) on Azimuthal Velocity (Vy) Contours at (a) N=100 rpm, (b) N=50 rpm.

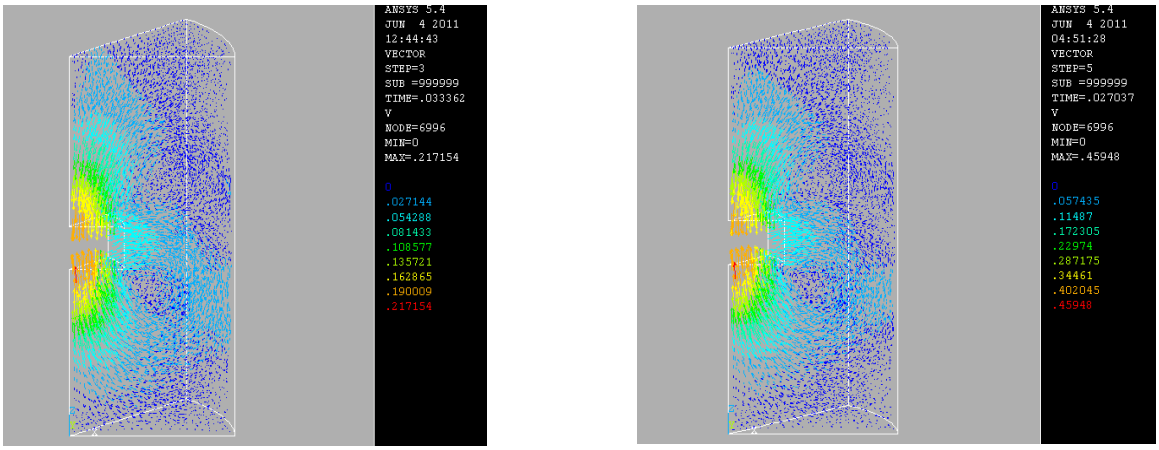

(a) (b)

Fig. 4. Effect of Rotating Speed (N) on Averaged Velocity Vectors Fields at (a) N=100 rpm, (b) N=50 rpm

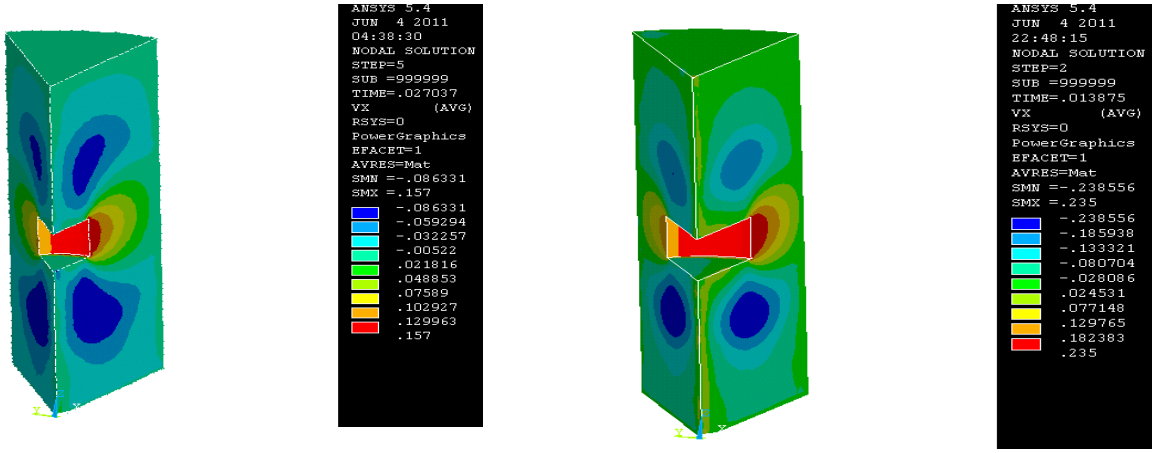

(a) **(b)**

Fig. 5. Effect of Impeller Diameter (D) on Radial Velocity Contours at ,(a) D= D /3 (b)D=D/ 2

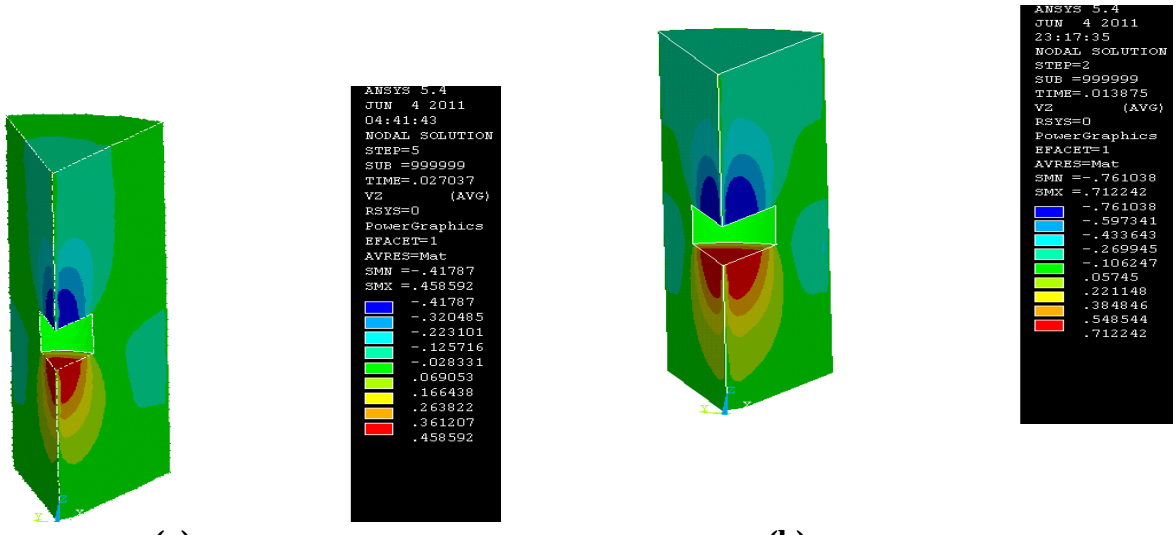

(a) **(b)**

***Fig. 6. Effect of Impeller Diameter (D) on Axial Velocity Contours at* , (a) D= D /3 (b)D=D/ 2.**

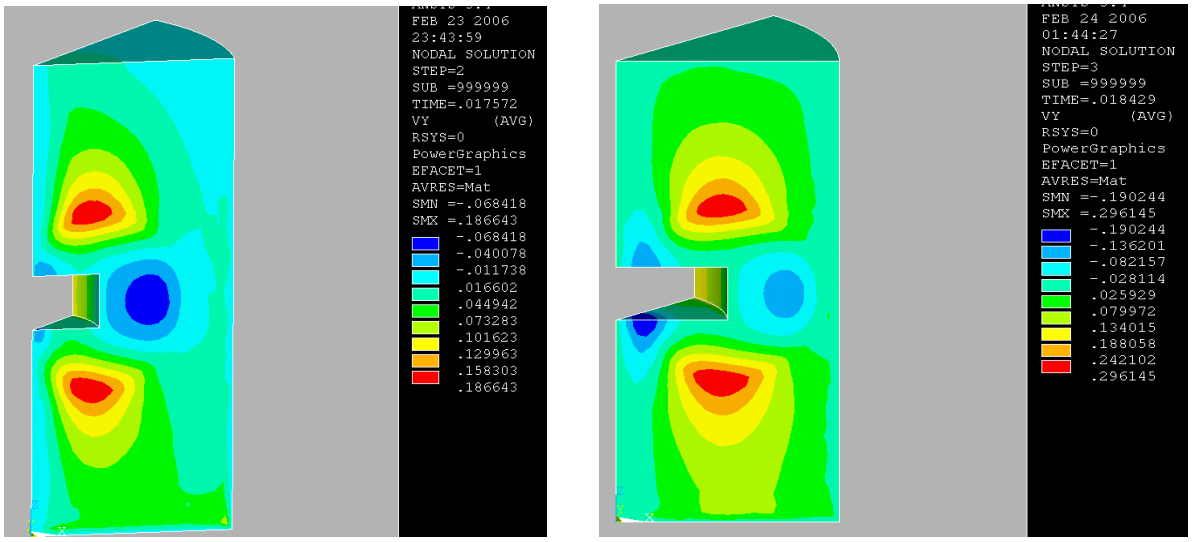

(a) ***(b)***

Fig. 7. Effect of Impeller DiameterD on Azimuthal Velocity Contours at ,(a) D=*D /3,(b D= D/2*

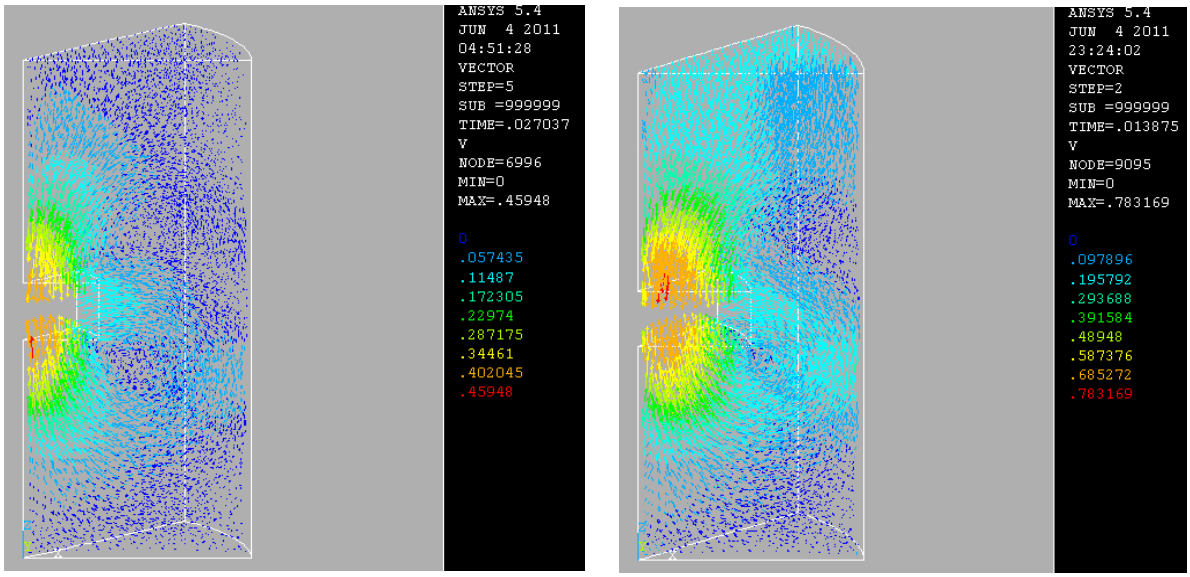

(a) (b)

Fig. 8. Effect of Impeller Diameter (D) on Velocity Vectors Fields at, ,(a) D=D /3,(b D= D/*2*

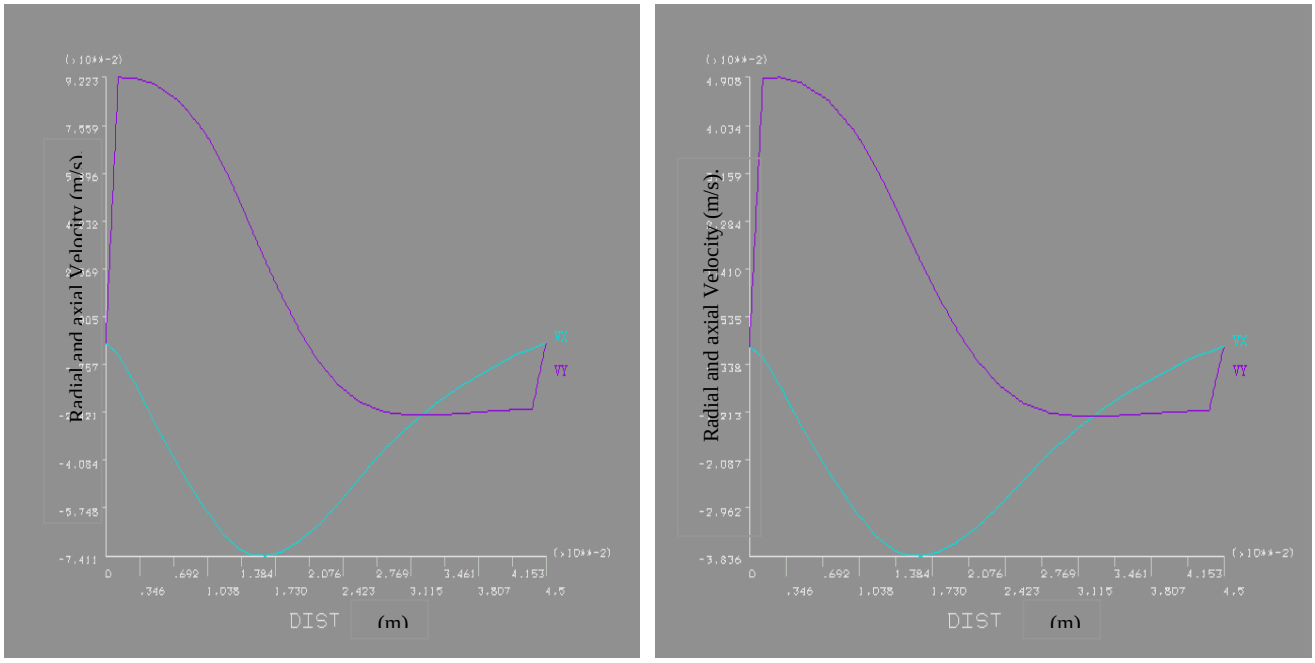

(a) (b)

Fig. (9): Effect of Rotating Speed (N) on Averaged Radial Velocity Profiles at Height 0.03m from the bottom of the tank, (a) N=100 rpm, (b) N=50 rpm.

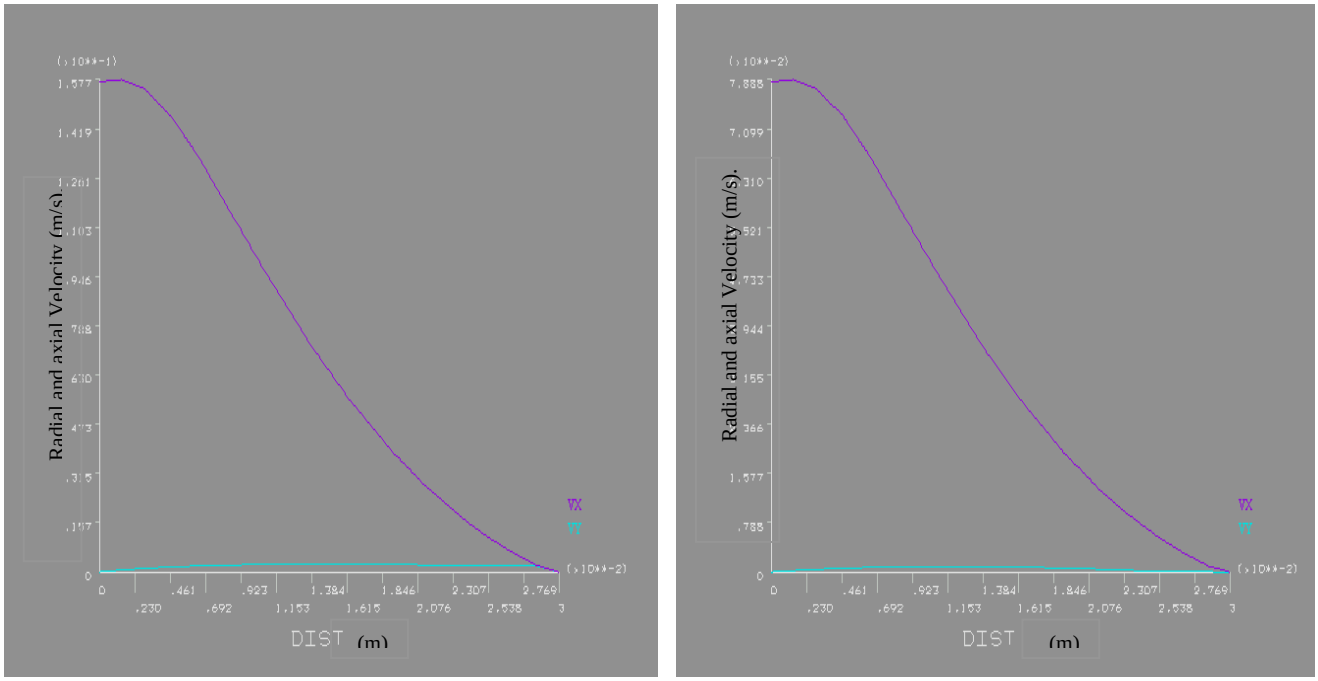

(a) (b)

Fig. (10): Effect of Rotating Speed (N) on Averaged Radial Velocity Profiles at Height y=0.052m From the Bottom of the Tank, (a) N=100 rpm, (b) N=50 rpm.

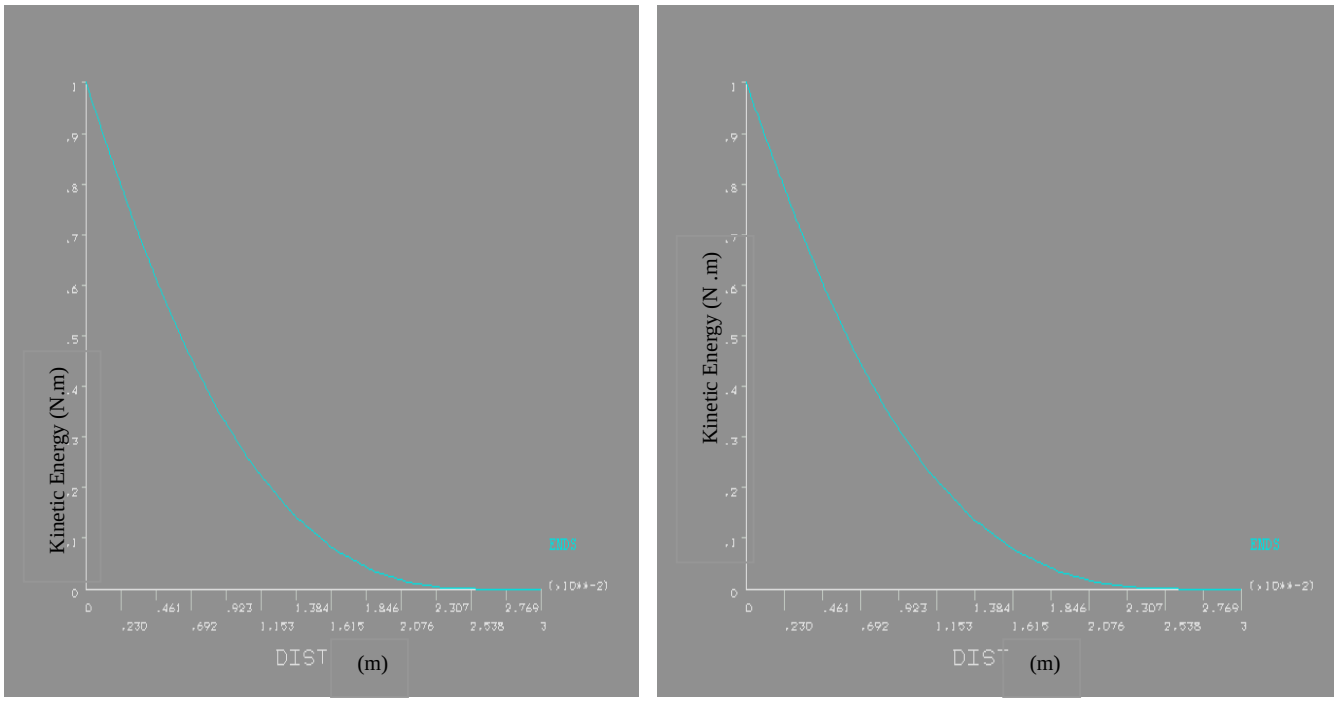

(a) **(b)**

Fig. (11) : Effect of Rotating Speed on Decay of Turbulence Kinetic Energy on Impeller Centerline at (a) N=100 rpm, (b) N=50 rpm.

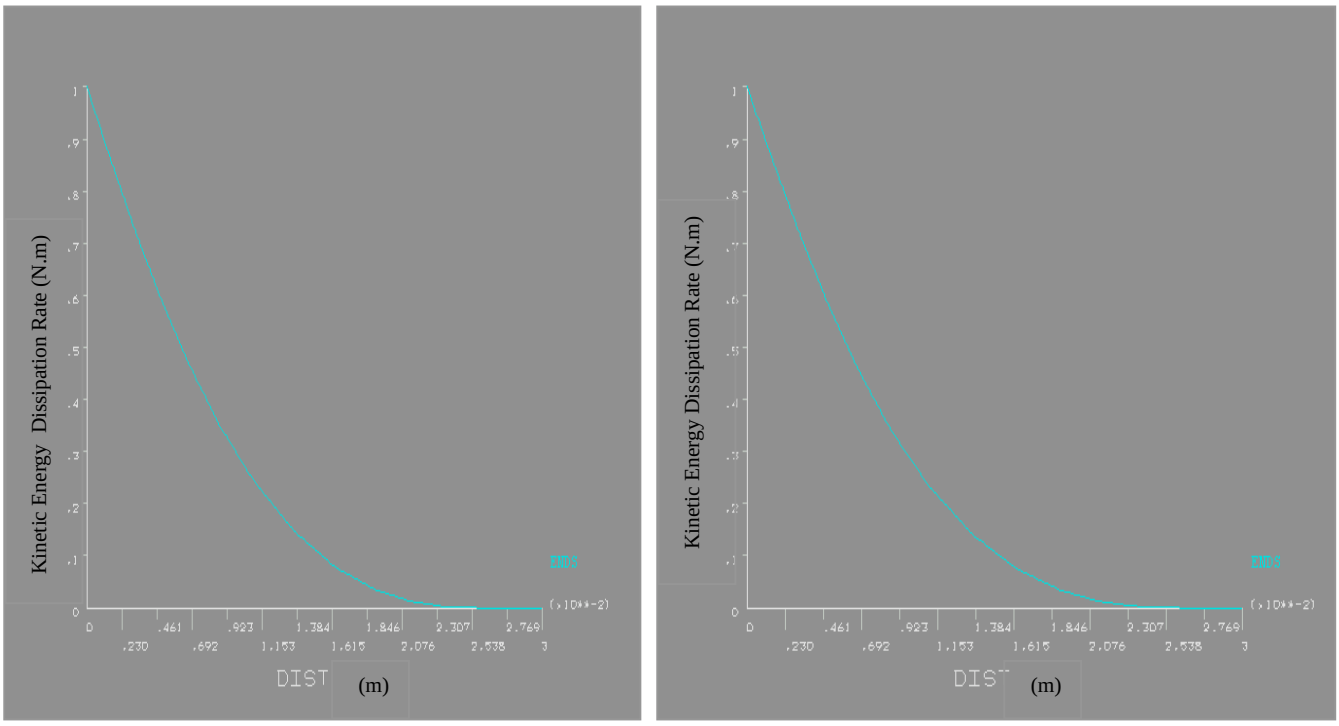

(a) **(b)**

Fig. (12): Effect of Rotating Speed on Decay of Turbulence Kinetic Energy Dissipation Rate on Impeller Centerline at ,(a) N=100 rpm, (b) N=50 rpm.

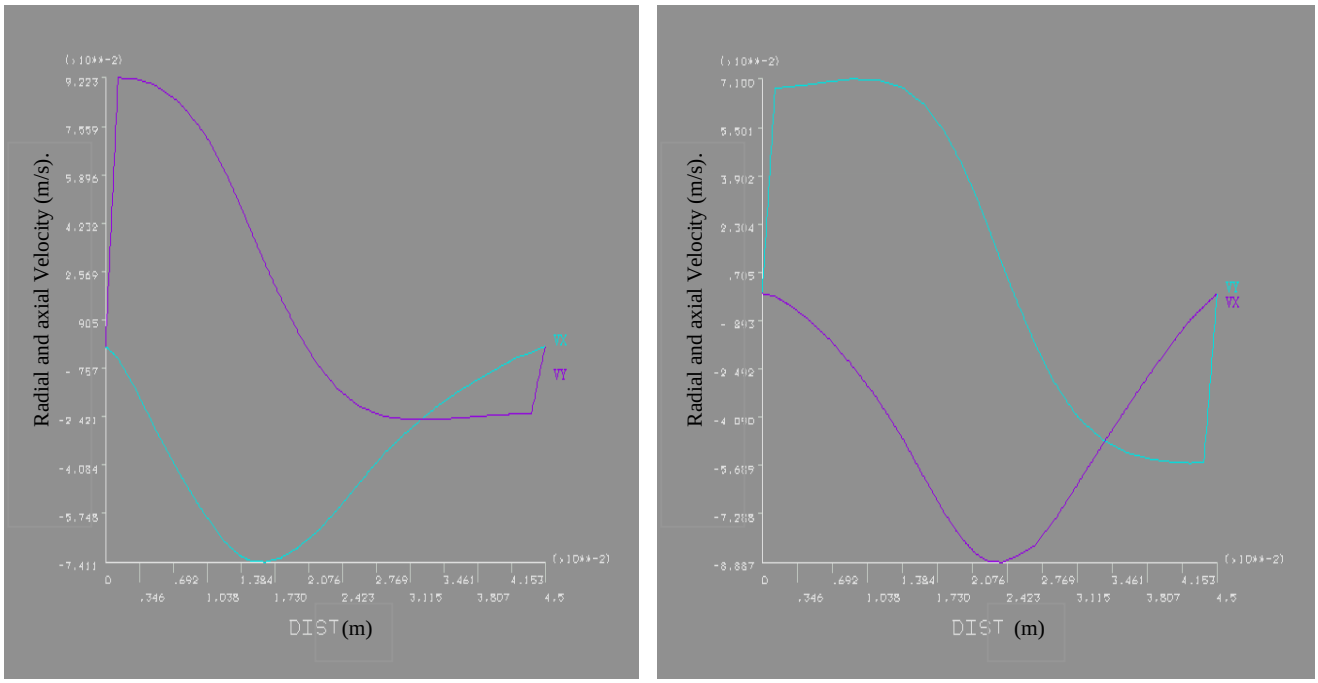

(a) (b)

Fig. (13) : Effect of Impeller Diameter (D) on Averaged Radial Velocity Profiles at Height y=0.03m $_T$, (b) D=D/3 $_T$ (a) D= D /2

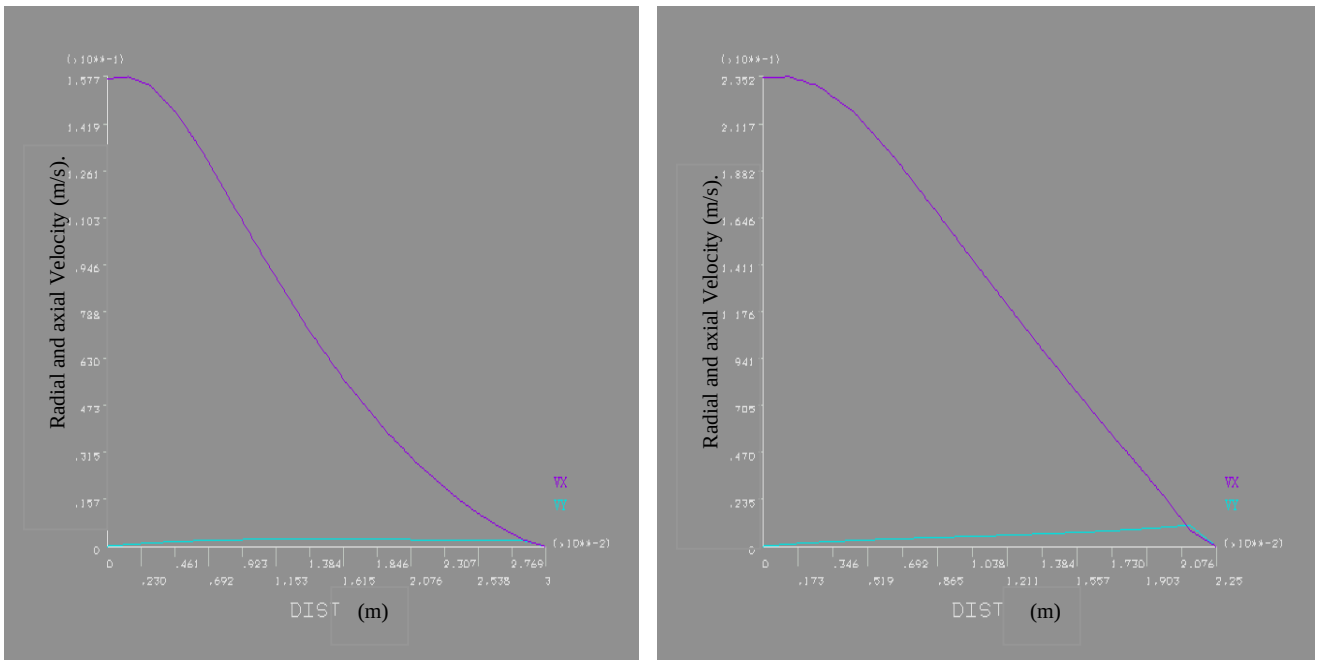

(a) (b)

Fig. (14) : Effect of Impeller Diameter (D) on Averaged Radial Velocity Profiles at Height y= 0.52m From the Bottom of the Tank, $_T$, (b) D=D/3 $_T$ (a) D= D /2

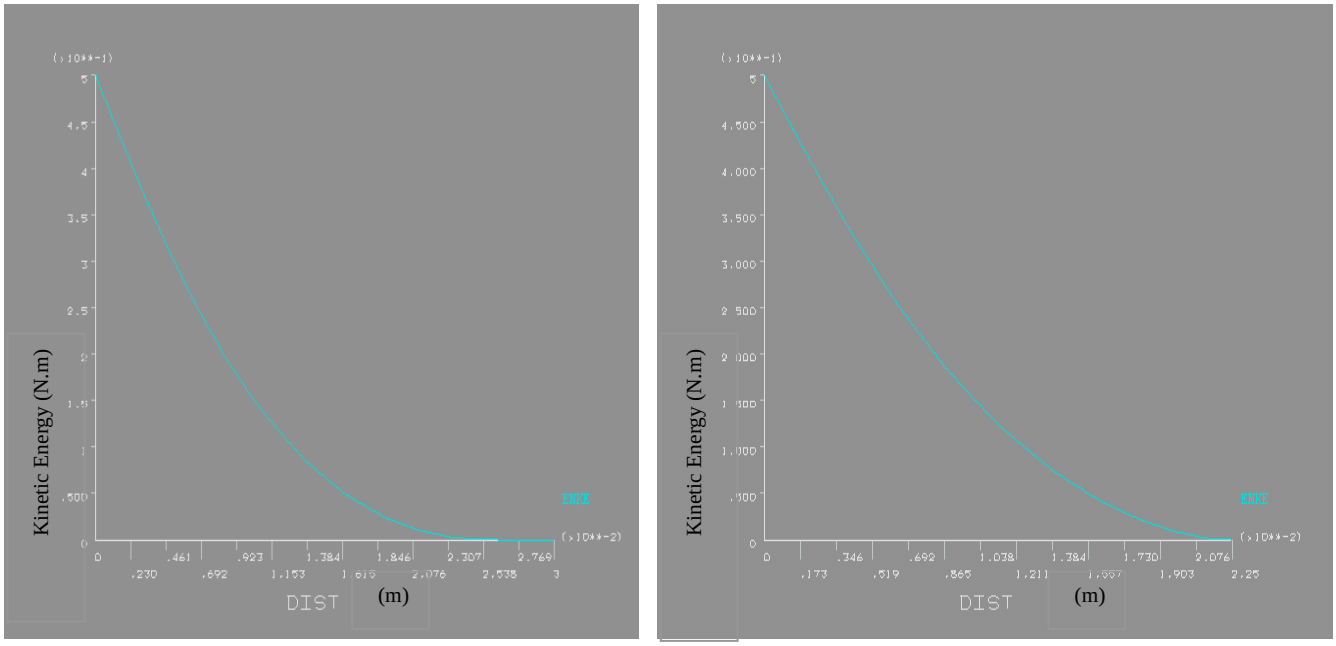

(a) **(b)**

Fig. (15): Effect of Impeller Diameter on Decay of Turbulence Kinetic Energy (a) D= D/2 (b)D=D/3

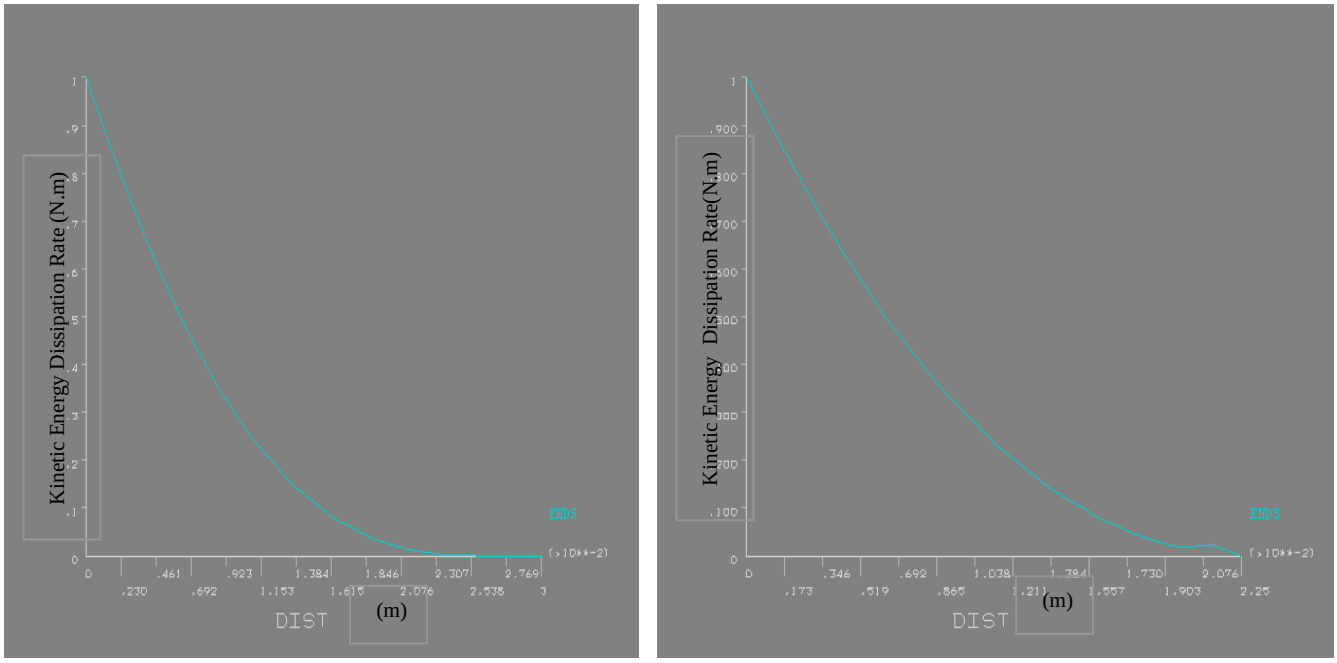

(a) (b)

Fig. (16) : Effect of Impeller Diameter on Decay of Turbulence Kinetic Energy Dissipation Rate(a) D= D/2 (b)D=D/3.

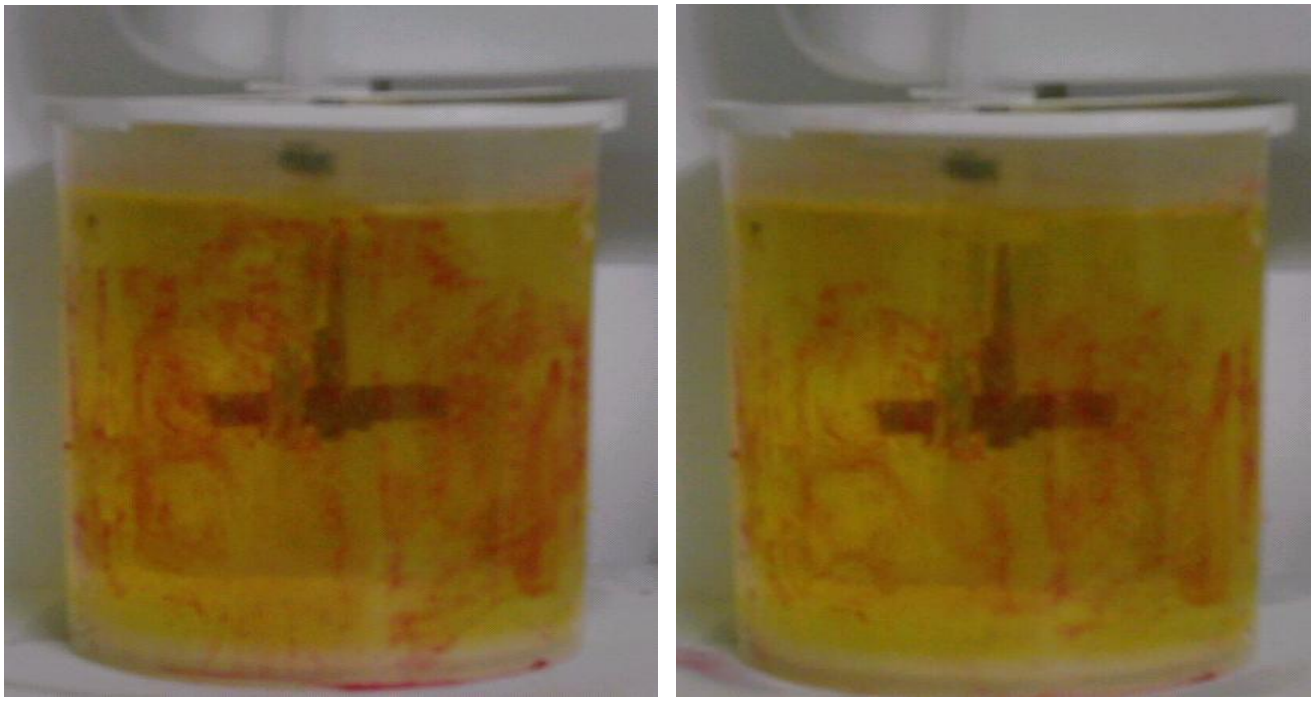

(a) (b)

Fig. (17): Effect of the Speed Reduction on the Colors Zones of the Acid-Base Visualization Method Test, (a) 100rpm and 0.04m Impeller Diameter, (b) 50rpm and 0.04m Impeller Diameter.

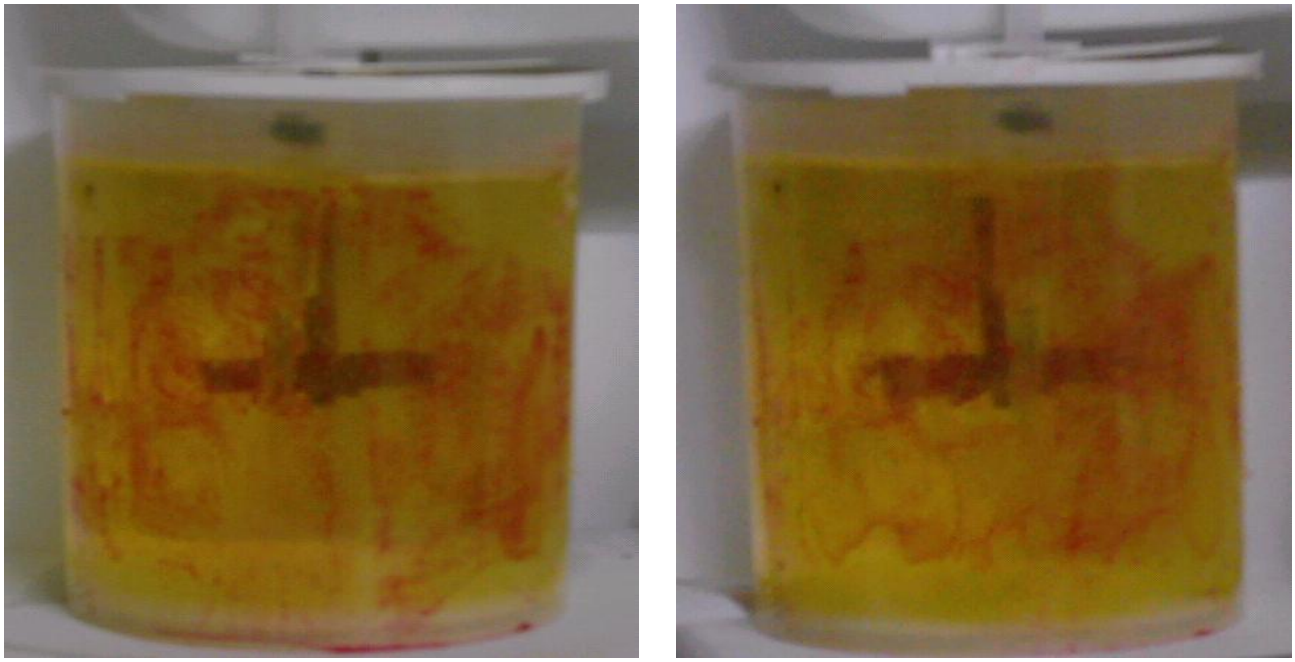

Fig. (18): Effect of the Impeller Diameter Increasing on the Colors Zones of the Acid-Base Visualization Method Test, (a) 100rpm and 0.04m Impeller Diameter, (b) 100rpm and 0.06m Impeller Diameter.

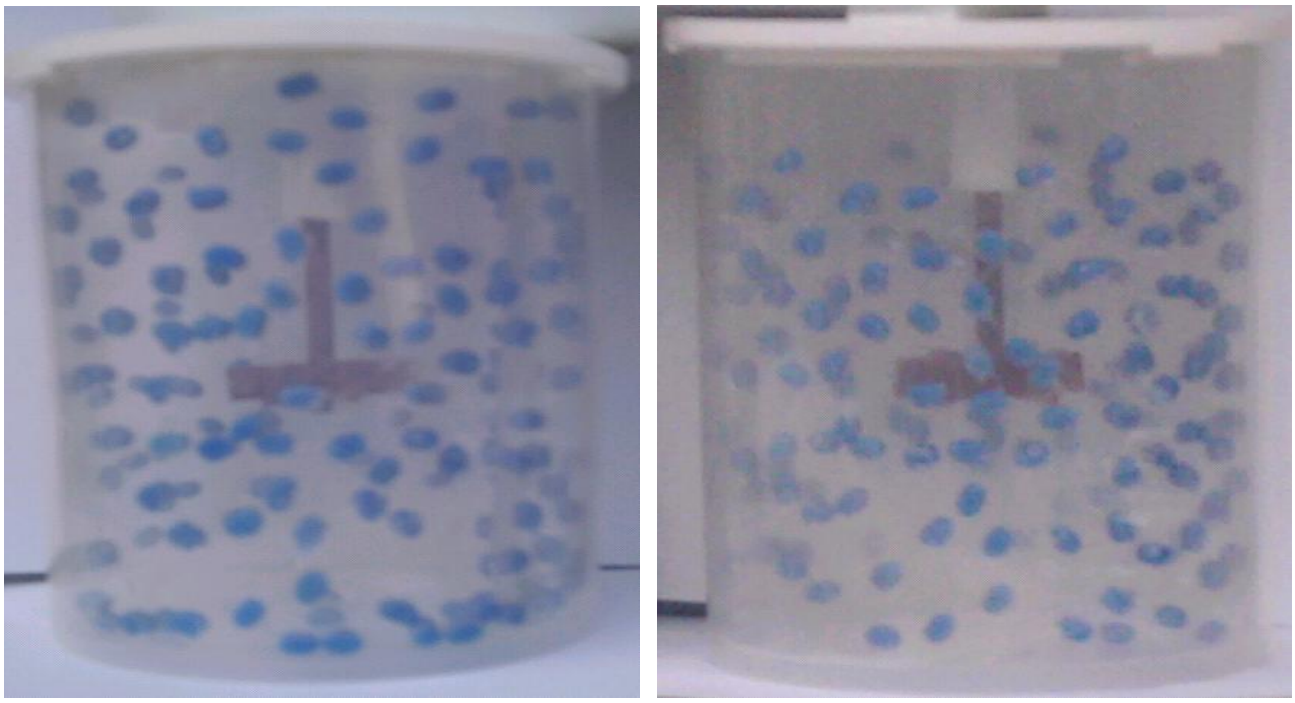

(a) (b)

Fig. (19): Effect of Speed Reduction on the Particles Distribution Visualization Test, (a) 100rpm and 0.04m Impeller Diameter, (b) 50rpm and 0.04m Impeller diameter.

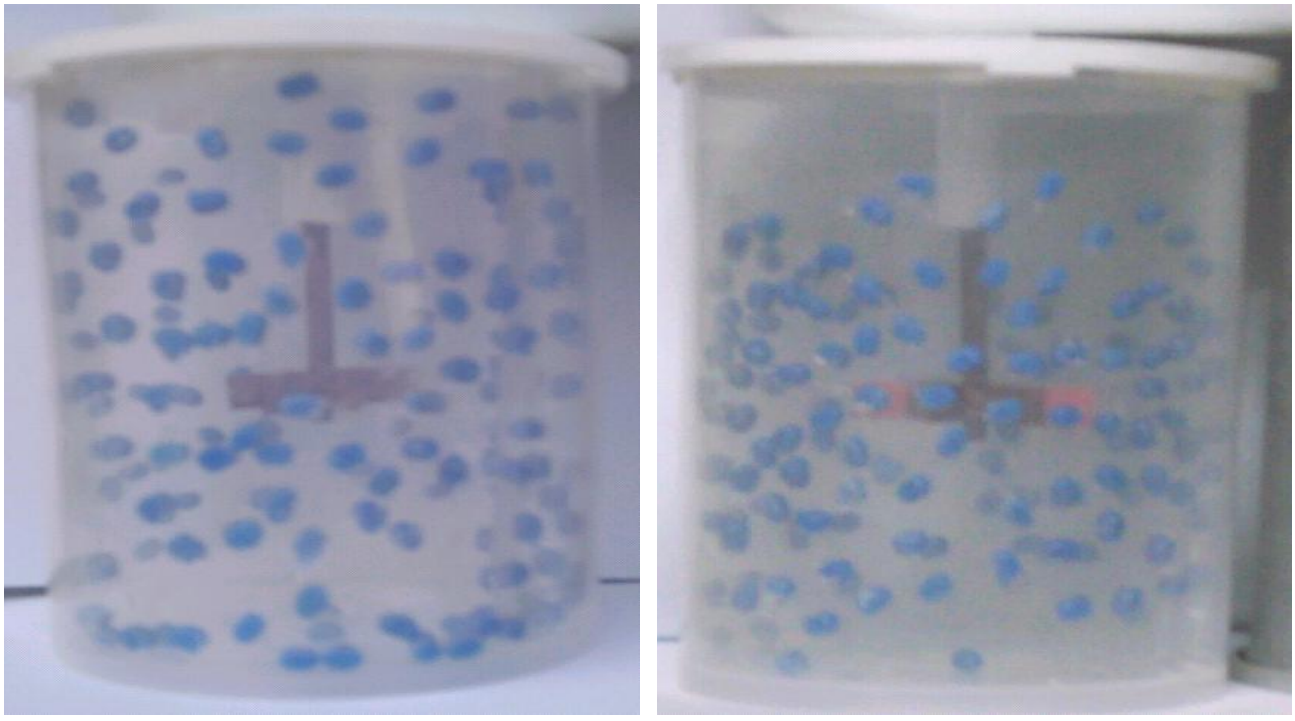

(a) (b)

Fig. (20): Effect of Impeller Diameter Increasing on the Particles Distribution Visualization Test, (a) 100rpm and 0.04m Impeller Diameter, (b) 100rpm and 0.06m Impeller Diameter